Int. J. Electrochem. Sci., 16 **(2021)** Article ID: 210636, doi: 10.20964/2021.06.54

International Journal of
ELECTROCHEMICAL
SCIENCE
www.electrochemsci.org

Deposition Mechanism and Corrosion Resistance of Ni-Graphene Composite Coatings Prepared by Pulse Electrodeposition

Bingying Wang[1], *Yongmin Zhao*[1], *Zhi Qin*[1], *Yige Liu*[1], *Enyang Liu*[1,*], *FengYang*[2], *Shouqin Li*[2]

[1] School of Materials Science and Engineering, China University of Petroleum (East China), Qingdao 266580, China
[2] Dongxin Oil Production Plant, Shengli Oilfield Company SINOPEC, Dongying 257094, China
[*]E-mail: enyangliu@126.com

Received: 16 February 2021 / *Accepted:* 10 April 2021 / *Published:* 30 April 2021

By adding graphene oxide (GO) to a Watt-type plating solution, a Ni-graphene (G) composite coating was prepared on a N80 steel substrate. Raman and FT-IR spectroscopy were performed to characterize the successful preparation and reduction of graphene oxide. The variation in the morphology of the composite coatings with changes in the average current density, rotation angle of cathode, and concentration of graphene oxide was examined using SEM and EDS analyses. An electrochemical corrosion test was used to study the effect of graphene oxide concentration on the corrosion resistance of composite coatings. A mechanism describing the action of the average current density and rotation angle of cathode during the codeposition process of Ni-G was proposed. It was found that the electrodeposition can be affected by the current density and rotation angle of cathode, confirming that the mechanism of Ni-G composite electrodeposition is controlled by both an electrochemical mechanism and a mechanical stirring mechanism. In addition, we proposed the mechanism of Ni-G composite electrodeposition.

Keywords: Ni-G composite coating; Pulse electrodeposition; Corrosion resistance; Deposition mechanism; Graphene oxide

1. INTRODUCTION

N80 steel pipes are widely used in petroleum drilling operations. However, due to the harsh environment [1] of steel pipes, corrosion is inevitable [2]. Corrosion has seriously affected the normal operation of petroleum systems and their production efficiency [3,4]. As a simple and economical method, electrodeposition is of interest and is widely used to improve the wear and corrosion resistance of N80 steel pipes [5-9]. Pulse electrodeposition is one of the most effective methods to prepare

composite coatings because the structure, wear resistance, porosity, and resistance can be better controlled by adjusting the pulse parameters. [10,11]. As early as 1843, R. Böttger proposed obtaining a nickel-based composite coating [12,13] by adding different nanoreinforcing phases; this coating can be used for metal corrosion protection due to its excellent mechanical properties and corrosion resistance [14-16]. Graphene (G) is a typical semimetal with a stable two-dimensional sp^2-hybridized crystal structure [15,17,18] and offers unique corrosion and wear resistance characteristics [19-21]. First, the theoretical Young's modulus of defect-free graphene sheets reaches 1.1 TPa. Due to the extremely high mechanical strength of graphene, the local deformation and wear loss of the material is reduced. Second, graphene is not easily penetrated by liquids and gases, so it can enhance the corrosion resistance of the material and reduce oxidation. [22,23]. Additionally, some scholars have compared the strengthening efficiency of different reinforcements introduced to nickel matrixes. It was shown that the Ni-graphite nanoplates and Ni-graphene [24-26] composites have the highest efficiencies, i.e., 188.4 and 124.2, are greater than those of other traditional reinforcements, such as SiC [27] particles, carbon fibers, and CNTs [28]. Therefore, graphene is an excellent reinforcing material for electrodeposited nickel (Ni) matrix composites. However, the graphene surface is hydrophobic, and the carbon skeleton is low polarity, which makes it difficult to disperse evenly in water. In the process of electrodeposition, due to the interaction between van der Waals forces and π - π stacking, graphene, with its large specific surface area, agglomerates in the bath, which affects the quality of electrodeposition. [22]. In contrast, graphene oxide (GO) not only has all the excellent properties of graphene but also contains many surface functional groups, such as hydroxyl, epoxy, carbonyl, or carboxyl groups. Such functional groups facilitate graphene oxide with better hydrophilicity and homogenized dispersion in the solution [29,30]. Moreover, studies have shown that a moderate addition of GO can improve the corrosion resistance of composite coatings [31], and the number of oxygen groups makes GO more compatible with the metal matrix [7, 32, 33]. However, graphene oxide is an insulator with many defects. Before codeposition with nickel ions, the oxygen-containing functional groups on the surface of graphene oxide combine with many metal ions to reduce the zeta potential [34, 35] and produce a large number of defects, resulting in many pores and holes on the surface of the coating, thus affecting the performance and quality of the coating. Consequently, the reduction of graphene oxide is widely used in electrodeposition [36]. In this paper, the functional groups on the graphene surface were modified and oxidized to form GO by an improved Hummers method, and then, GO was reduced by pulse electrodeposition to obtain a better Ni-G composite coating. At present, few studies have been published on the mechanism of codeposition of G with nickel. Guglielmi N. et al. proposed a two-step adsorption theory for the codeposition process in composite electrodeposition [37]. This theory holds that when particles co-deposit with metals, first, the particles are covered by adsorbed ions and solvent molecules, forming a weak adsorption layer under the action of van der Waals forces. Subsequently, the particles, which absorbed various metal ions, move to the cathode under the action of the electric field. When the particles electrophorese to the double layer, there is relatively strong adsorption between particles and the cathode due to the increased electrostatic attraction. This process is called strong adsorption. The model was well validated in Ni-SiC [38], Ni-Al_2O_3 [39], Ni-WC [40], and other systems. The electrochemical mechanism [41] suggests that composite electrodeposition depends critically on the charge transfer between the electrode and the bath. There are some main points: the process of composite electrodeposition was determined by the migration

rate of particles and the formation of electrostatic adsorption on the electrode surface. Snaith, D W et al. [42] proposed another hypothesis that the electrophoretic velocity of the solid particles in the bath was negligible compared with that of mechanical stirring. The dispersed particles were brought to the surface of the cathode via mechanical stirring. As the metal coating continuously thickened, the particles dispersed in it. Only a few particles were fixed due to the reduction of the surrounding metal ions, while the majority of the particles were washed down due to the tangential force.

The above mechanisms clearly explain the composite electrodeposition from different angles. The joint control of the electrochemical mechanism and the mechanical stirring mechanism is more suitable for the exploration of the composite electrodeposition mechanism; this idea is explored in this paper.

2. EXPERIMENTAL

2.1 Electrodeposition of Ni-G composite coating

GO was obtained by a modified Hummer's method. Ni-G composite coatings were deposited using pulse electrodeposition. The pulse on time (T_{on}) was 2 ms, and the pulse (T_{off}) was 3 ms. The watt plating solution consisted of 250 g/L $NiSO_4$•$6H_2O$, 40 g/L $NiCl_2$•$6H_2O$, 30 g/L H_3BO_3, 2 g/L saccharin sodium, 0.2 g/L $C_{12}H_{25}SO_4Na$, and 0.2~1 g/L graphene oxide and was used to fabricate the samples at 60℃. The pH of the bath was maintained at approximately 4~5. The duration of the electrodeposition was 2 h. To explore the influence of process parameters on electrodeposition, the range of current density was 0.5~2 A/dm^2, and the range of rotation angle of cathode was 0~90°.

2.2 Characterization and measurements

Raman spectra of the GO and Ni-G composite coatings at 1.5 A/dm^2 were obtained on a DXR Raman spectrometer with a wavelength of 532 nm and power of 5 mW as an excitation source, and the Fourier transform infrared (FT-IR) spectra were obtained on a Nicolet IS50 FT-IR spectrometer with a resolution of 4 cm^{-1}. Moreover, the microstructure of the composite coating and the cross-section were observed by scanning electron microscopy (SEM, Nova Nano SEM450), and the content of elements contained in the coatings was measured by energy-dispersive X-ray spectroscopy (EDS). The corrosion resistance of the composite coating in 3.5% NaCl was studied using standard techniques such as electrochemical impedance spectroscopy and potentiodynamic polarization. The electrochemical impedance test was carried out in the frequency range of 10^{-2}~10^5 Hz, and the AC amplitude was 10 mV. The potentiodynamic polarization was measured by scanning from −500 mV to 500 mV at a rate of 1 mV/s.

3. RESULTS AND DISCUSSION

3.1 Characterization of graphene oxide

Fig. 1 shows the Raman spectrum of the composite coating. The G peak strength in the Raman spectrum of carbon nanomaterials represents the quantity and integrity of the aromatic ring structure in GO, while the D peak strength represents the disorder of the GO structure caused by the destruction of the aromatic ring structure in GO during the oxidation process.

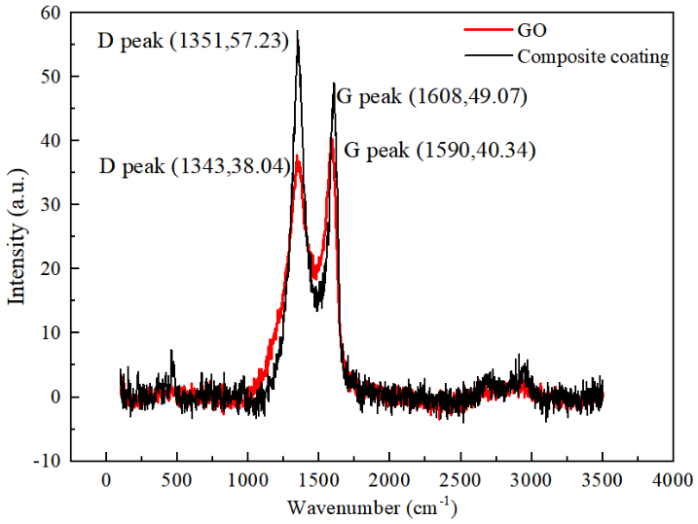

Figure 1. Raman spectra of the GO and Ni-G composite coatings electrodeposited at 1.5 A/dm^2.

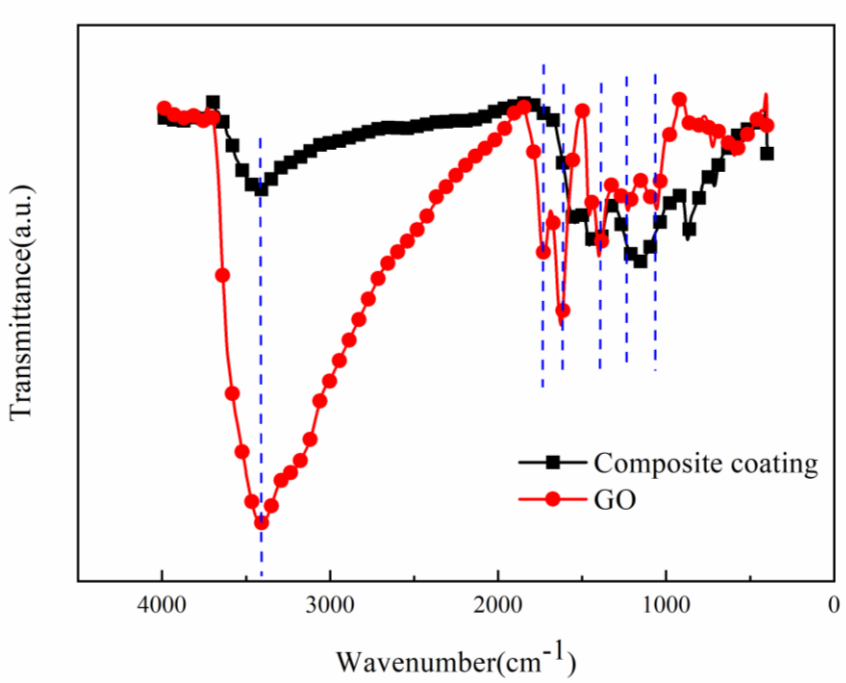

Figure 2. FTIR spectrum of the Ni-G composite coating electrodeposited at 1.5 A/dm^2 and GO.

The intensity ratio of the D and G peaks (I_D/I_G) is usually used to evaluate the graphitization degree of nanocarbon materials. The smaller the ratio (I_D/I_G) is, the higher the reduction degree of graphite. Singh et al. [43] found that the G peak of GO was wide and strong at 1598 cm^{-1} in the Raman spectrum of GO. And the oxygen-containing functional groups such as carboxyl group, hydroxyl group and epoxy group were found in the FT-IR spectrum of GO. All that indicate a few layer-GO is actually synthesized. In our work, the Raman spectrum of GO is shown in Fig. 1. The G band of GO shows a wide, strong band at 1590 cm^{-1} because the sp^2 graphite skeleton is deformed due to the attachment of oxygen-containing functional groups. The FT-IR spectrum of GO is shown in Fig. 2. In the spectrum, the hydroxyl (-OH) and alkoxy (RO-) vibration absorption peaks are at 3448 cm^{-1} and 1067 cm^{-1}, the carbonyl (-C=O) and epoxy (C-O-C) stretching vibration absorption peaks are at 1724 cm^{-1} and 1239 cm^{-1}, respectively. This spectrum shows that graphene oxide was successfully prepared [44]. As shown in Fig. 1, the D and G peaks appear at 1343 cm^{-1} and 1590 cm^{-1} in the Raman spectrum of GO, and it can be calculated that the I_D/I_G ratio is 1.06. The D and G peaks appear at 1351 cm^{-1} and 1608 cm^{-1} in the Raman spectrum of the Ni-G composite coating, and the I_D/I_G ratio dropped from 1.06 to 0.86. This decrease in the ratio represents the decrease in disordered domains that occurs during GO reduction. Compared with the peak intensity in the infrared spectrum of graphene oxide, as shown in Fig. 2, the intensity of each characteristic peak of the composite coating decreased, especially the vibration absorption peak of hydroxyl (-OH) groups at 3448 cm^{-1}. This indicates that the number of oxygen-containing functional groups on the surface of graphene oxide decreases and is gradually reduced in the process of composite electrodeposition.

3.2 Morphology of the composite coating

3.2.1 Effect of current density on the morphology of the composite coating

Fig. 3 shows the surface and cross-sectional morphology of the composite coating at different current densities. The specific change in coating thickness is shown in Fig. 4. Guo et al. [45] described that that the surface of the composite coatings became coarser as the current density increased. It is generally believed that the morphology of the composite coatings is significantly affected by the change in current density.

When the current density was 0.5 A/dm^2 (as shown in Fig. 3a), a series of sparse cellular protuberances appeared on the coating surface. The corresponding cross-section of the surface has more protrusions and low flatness, and the thickness is relatively low, only 18.9 μm. With increasing current density, the morphology of the coating surface changed obviously. The cellular bulges became more homogenized, the size of cellular protuberances on the entire coating became small and dense, and the surface two-dimensionality and the thickness of the corresponding cross-section improved. The Ni-G composite coating prepared at a current density of 1.5 A/dm^2 possessed the smallest and densest cellular protuberances, as shown in Fig. 3c. This means that an increased current density led to a more uniform and compact coating morphology. An appropriate increase in the current density increases the number of electrons supplied to the cathode and the degree of cathode polarization. Therefore, the cathode overpotential was increased simultaneously, which increased the nucleation rate of the cathode surface

and the density of the coating. The results showed that when the current density exceeded 1.5 A/dm^2 (Fig. 3d), the surface of the coating was not uniform and the cellular structure was fuzzy and irregular.

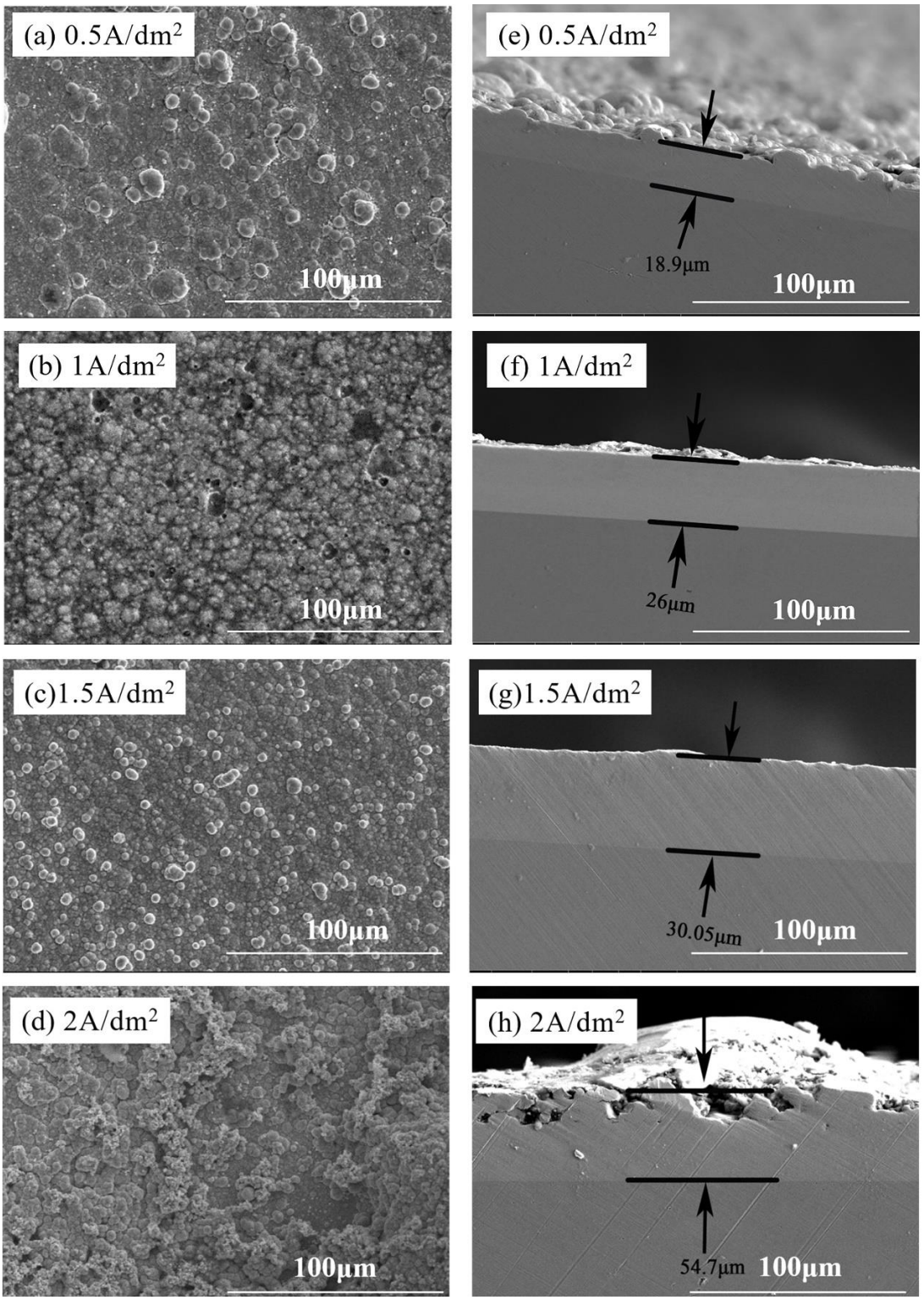

Figure 3. Surface and cross-sectional morphology of the Ni-G composite coatings electrodeposited at different current density 0.5 A/dm^2 (a, e), 1 A/dm^2 (b, f), 1.5 A/dm^2 (c, g), 2 A/dm^2 (d, h).

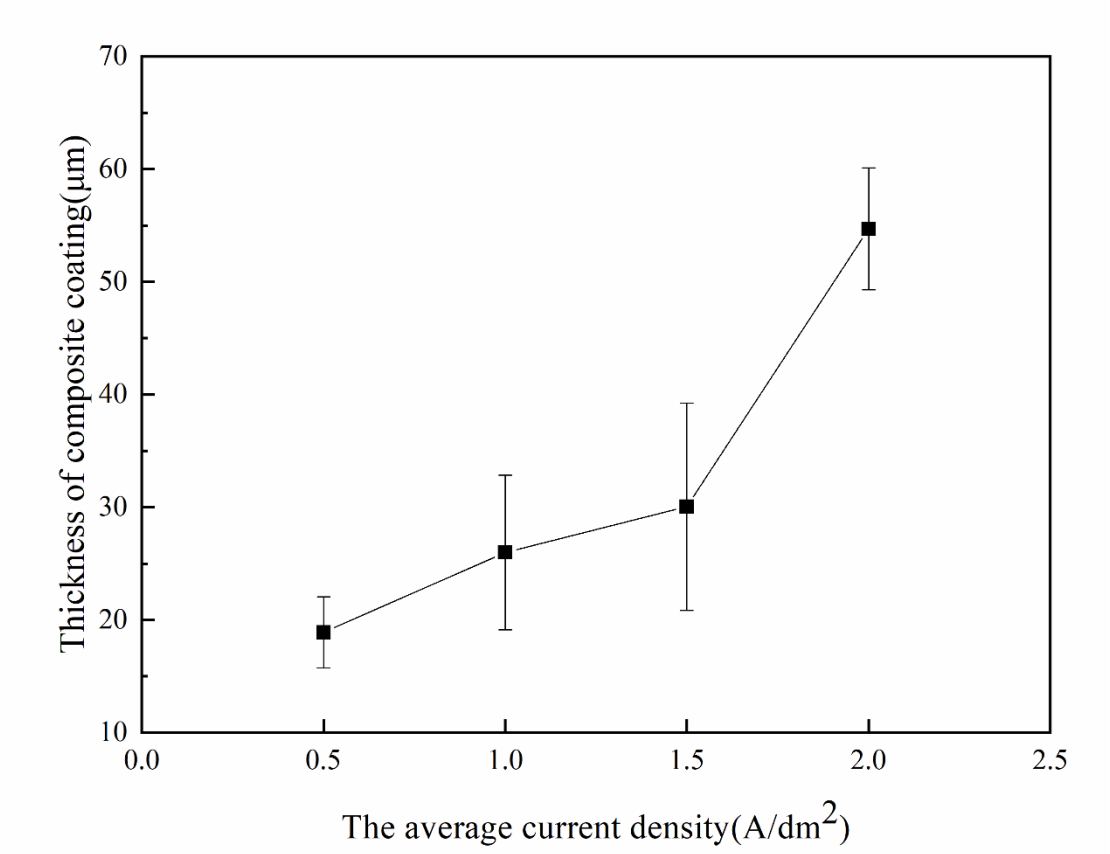

Figure 4. Thickness of the Ni-G composite coatings electrodeposited at different current density (0.5 A/dm^2, 1 A/dm^2, 1.5 A/dm^2, 2 A/dm^2).

The reason is that the reduction rate of nickel ions and graphene oxide increases with increasing current density, which makes the functional groups on the surface of graphene oxide gradually detach, the hydrophobicity of graphene oxide decreases, and the agglomeration increases [46]. Therefore, the current density has been found to be effective in the deposition of Ni-G composite coatings, which verifies the adaptability of the electrochemical mechanism.

3.2.2 Effect of rotation angle of cathode on the morphology of the composite coating

Huang et al. [47] studied the influence of cathode Surface velocity on Friction. Experiments show that a moderate flow rate of the plating solution on the cathode surface is beneficial to the formation of defect-free nickel films. This is related to the rotation angle of cathode. Chernyshev et al. [48] simulated the electrocrystallization of copper, zinc, and other particles to prepare ultra-thin films on a rotating cathode. The model used can predict the effect of the electrolysis conditions on the sediment structure at low electrolysis times and pulse modes. Therefore, it is of great significance to study the effect of rotation angle of cathode on the electrodeposition.

The surface morphology of composite coatings with different rotation angle of cathode is shown in Fig. 5. The number of particles on the coating increases gradually with increasing cathode angle from 0° to 90° in the electroplating bath. As shown in Fig. 6, the percentage of C atoms is low (34.93%) when

the cathode angle is 0°, whereas the cathode angle of 90° achieves the maximum C percentage of 82.06. That is, the atomic percentage of C was largely enhanced after increasing the cathode angle, and the growth rate increased gradually. The trend of the change in weight percentage of C is similar to that of the change in atomic percentage, which further confirms that the increasing the cathode angle accelerates the composite electrodeposition. When the bath flows in the direction of electromagnetic stirring, certain forces work upon the cathode surface; these forces include adhesive forces favorable to electrodeposition and scouring forces unfavorable to electrodeposition. When the cathodic current flows in the same direction as the plating solution (i.e., the cathode angle of 0°), the scouring force is far greater than the adhesion; therefore, the number of particles deposited on the surface of the coating is very small, as shown in Fig. 7(a). In Fig. 7(b)~(d), it is seen that the adhesion of the plating solution on the cathode surface was evidently elevated after the cathode angle increased. However, the scouring force decreased gradually. Hence, the number of particles deposited on the coating surface was largely enhanced. When the cathode angle was 90°, the adhesive force on the cathode surface reached the maximum, the number of particles deposited on the coating surface was the largest, and the density of the coating reached the maximum.

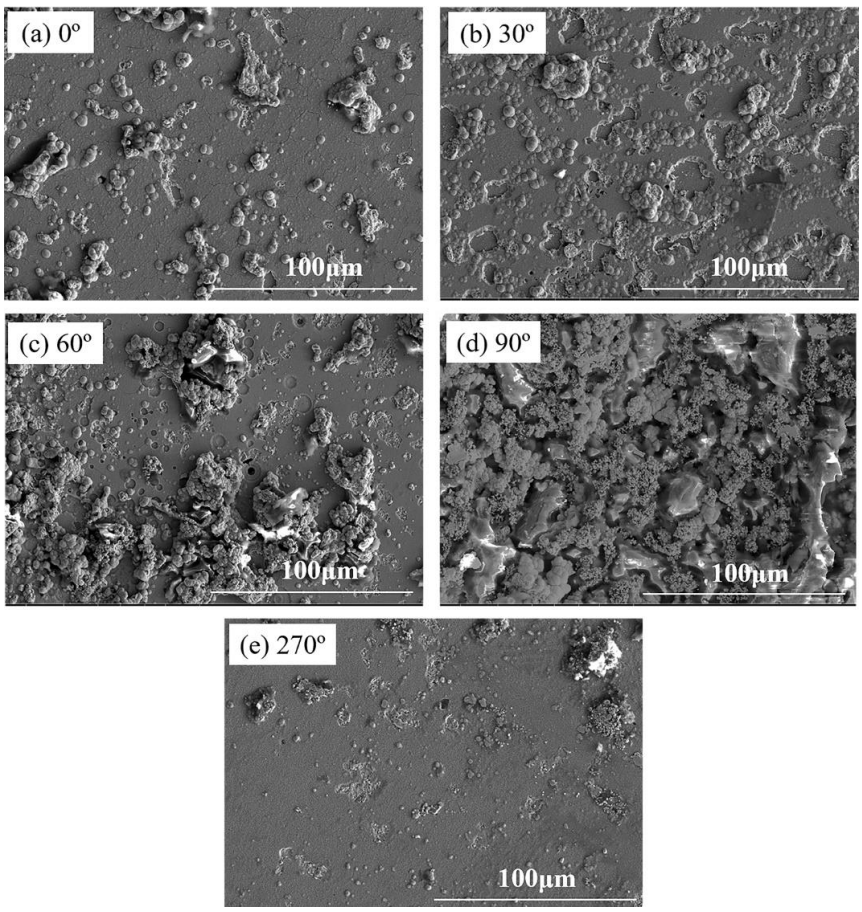

Figure 5. Surface morphology of the Ni-G composite coatings prepared at different angles of cathode prepared at 1.5 A/dm^2. (a) 0°, (b) 30°, (c) 60°, (d) 90°, (e) 270°.

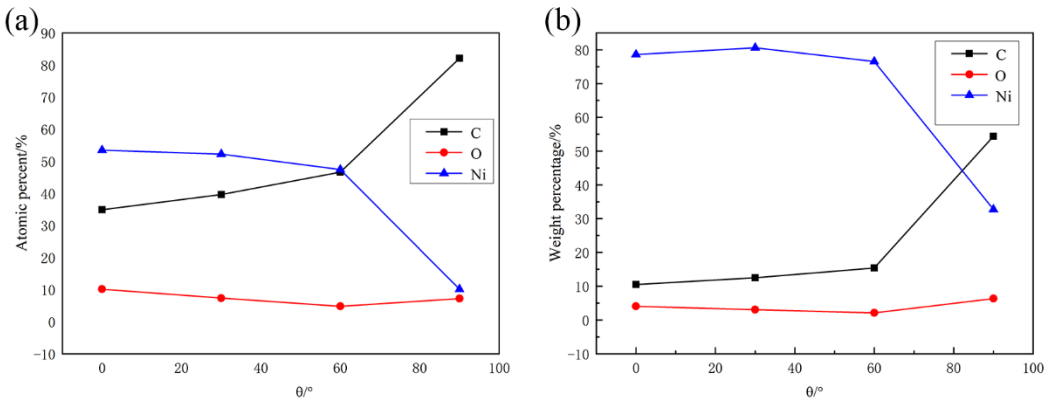

Figure 6. (a) Atomic percentage of the elements in the Ni-G composite coating at different rotation angle of cathode and (b) weight percentage of the elements in the Ni-G composite coating at different rotation angle of cathode prepared at 1.5 A/dm^2.

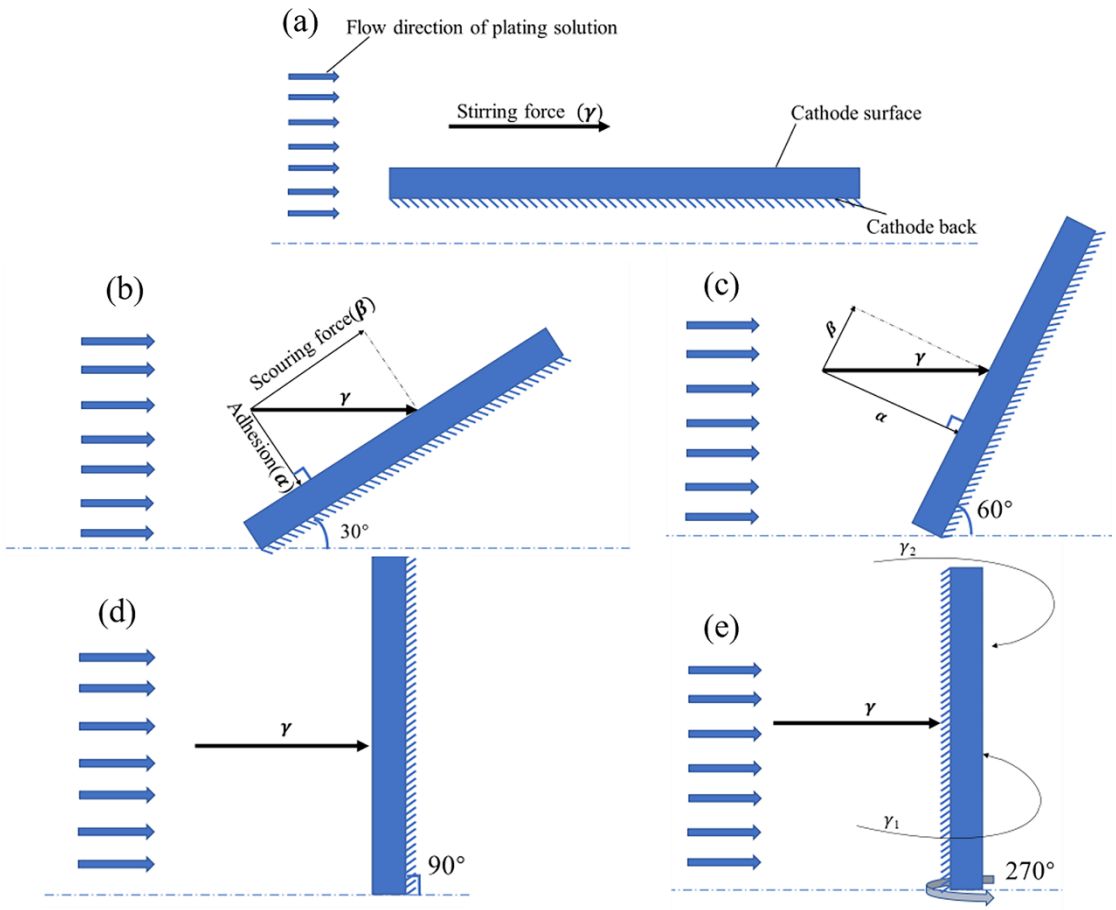

Figure 7. Schematic diagram of the Ni-G composite coating deposition mechanism with different rotation angles of cathode.

Moreover, when the surface of the coating returned to the flow direction of the bath, a few particles were still observed on the surface. This is because the plating solution flows around the back of the coating when it flows through the sample, forming a vortex (Fig. 7e).In summary, appropriately

increasing the rotation angle of cathode has a positive effect on the deposition of the Ni-G composite coating. This indicates that Ni-G composite electrodeposition conforms to the mechanical stirring mechanism.

3.2.3 Effect of graphene oxide content on the morphology of the composite coating

Karim et al. showed that, with the increase of graphene oxide concentration, the surface roughness of the coating increases. When the concentration of graphene oxide is 0.2 %, the surface roughness of the coating reaches the maximum [49] It is generally believed that the morphology of the composite coatings is significantly affected by the concentrations of graphene oxide.

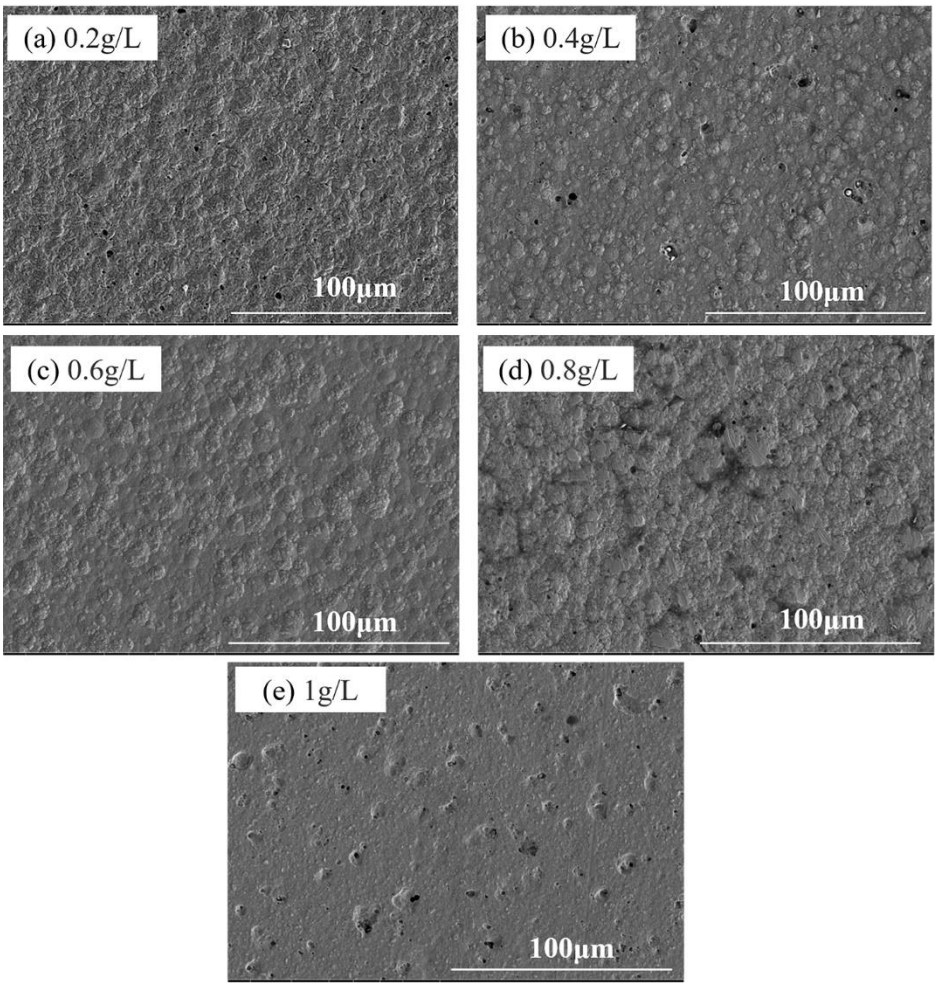

Figure 8. Surface morphology of the Ni-G composite coatings with different concentrations of graphene oxide prepared at 1.5 A/dm^2. (a) 0.2 g/L, (b) 0.4 g/L, (c) 0.6 g/L, (d)0.8 g/L, (e) 1 g/L.

By adding different concentrations of graphene oxide to the basic plating solution, the surface morphology of the composite coating was obtained by electrodeposition (Fig. 8). It can be seen from the figure that when the concentration of graphene oxide was 0.2 g/L ~ 0.4 g/L, the surface morphology of

the composite coating was rough and had a needle-hole structure. As the concentration of graphene oxide increased, the surface of the composite coating became dense and uniform, as shown in Fig. 8(d), but when the concentration of graphene oxide exceeded 0.6 g/L, it became irregular. This behavior is due to the addition of nanoparticles; as nanoparticles are added, the microstructure of the composite coating becomes fine and uniform, and the number of cell protrusions and cracks gradually decreases [50]. However, when too many nanoparticles are added, agglomeration occurs, which reduces the uniformity of the coating structure and causes it to coarsen [51,52]. In the electrodeposition process, as the content of GO increases, the content of reduced graphene gradually increases. The pinhole defects are continuously filled by reduced graphene and nickel metal, which are densely and uniformly deposited on the cathode plate. However, when the concentration exceeds a certain range, the graphene oxide cannot disperse completely in the solution, causing extensive agglomeration, and instead, the coating surface becomes rough.

3.3. Ni-G co-deposition mechanism

The deposition process of the Ni-G composite coating can be explained by the model shown in Fig. 9. The analysis is as follows: first, water molecules can combine with the free nickel ions in the plating bath through the solvation process due to their dipole characteristics to form a positively charged hydrated nickel ion surrounded by six water molecules; the reaction equation is as follows: $Ni^{2+}+H_2O\rightarrow[Ni(H_2O)_6]^{2+}$. Under the action of the positive and negative charges and the external electric field, suspended negatively-charged GO sheets adsorb hydrated ionic nickel complexes, which migrate to the diffusion layer near the cathode due to mechanical stirring and electrostatic attraction. Subsequently, the composite particles enter the Helmholtz double layer from the diffusion layer near the cathode surface. This process is affected by the high electric field intensity. Hence, the hydration layer is removed from the hydrated nickel ion in this process. Then, one end of the GO sheet, which has a large number of nickel particles on the surface, moves toward the cathode and makes contact with it. Due to the superconductivity of GO, it can immediately carry out electronic exchange with the cathode surface to achieve a reduction reaction. Some studies have shown that the reduction peak of GO on the electrodeposition curve does not move with the change in pH, which means that H^+ is not involved in the reduction of GO, so the reduction equation can be written as: $GO + ne^-\rightarrow G$ [53]. With the flow direction generated by the stirring force, the other end of the GO is connected to another position of the substrate for reduction. At the same time, the nickel ions removed from the hydration layer also make contact with the cathode for electron exchange to promote a reduction reaction, and the reaction formula is as follows: $[Ni(H_2O)_6]^{2+}+2e^-\rightarrow Ni+6H_2O$. Thus, co-deposition of G and Ni atoms on the cathode surface is achieved.

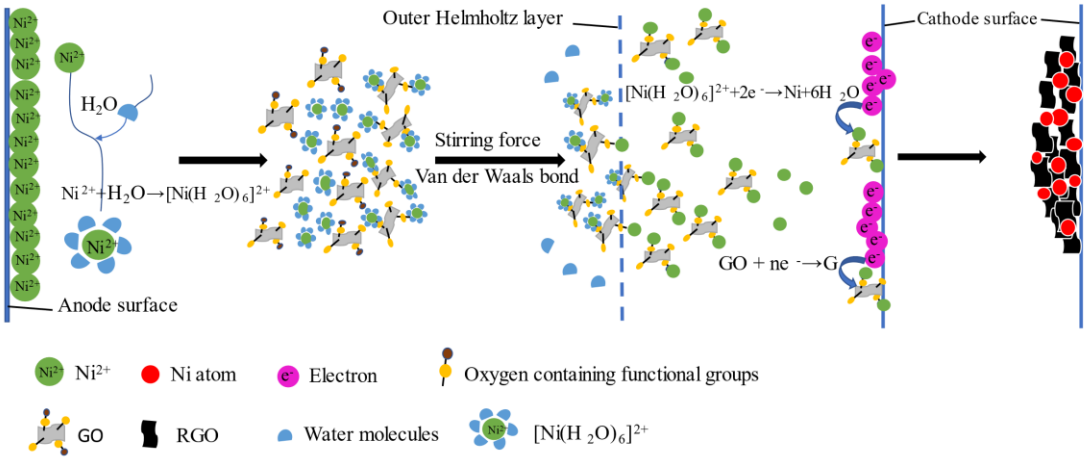

Figure 9. Model of the Ni-G composite deposition.

3.4. The corrosion resistance of the composite coating

The polarization curve of the composite coating under different graphene oxide concentrations is shown in Fig. 10. The vertical axis is the potential, and the horizontal axis is the logarithm of the absolute current. Fitting the polarization curve to obtain the corresponding Tafel slope, the self-corrosion potential (E_{corr}) and self-corrosion current density (i_{corr}) are shown in Table 1. Among them, E_{corr} reflects the difficulty of corrosion in terms of thermodynamics, and i_{corr} characterizes the speed of corrosion in terms of dynamics. Generally, the lower the self-corrosion potential is, the more likely the material is to be corroded; the lower the self-corrosion current density is, the better the corrosion resistance of the material.

Fig. 10 and Table 1 show that the self-corrosion current density of the pure nickel coating is significantly higher than that of the nickel coating with graphene oxide. With increasing graphene oxide concentration, the E_{corr} of the coating increases, the i_{corr} decreases, and the corrosion tendency and corrosion rate of the coating decrease obviously. When the concentration of graphene oxide in the bath is 0.6 g/L, the i_{corr} reaches the lowest value, which is 5.14×10^{-7} A/cm^2, and the corrosion resistance of the coating reaches the maximum. As the concentration of graphene oxide continues to rise, E_{corr} and i_{corr} increase, which indicates that the corrosion tendency increases and the corrosion resistance of the coating worsens. This is because an excessive concentration of graphene oxide increases the number of defects in the coating and increases the contact area between the corrosion medium and the coating surface, resulting in a decrease in the corrosion resistance of the coating. Min et al. [54] studied the corrosion resistance of Ni-Co composite coating in 1 mol/L hydrochloric acid solution. The results show that the polarization curve of the composite coating reaches the maximum when the concentration of rare earth is 0.25g/L. Zhang et al. [55] showed the corrosion resistance of Cu/Ni–P composite coating obtained at pH 2.0, Dk = 8.0 A/dm^2 in 3.5% NaCl solution. Compared with the substrate, the corrosion resistance of the electrodeposited composite coating is obviously improved, this is consistent with our research on the corrosion resistance of composite coatings.

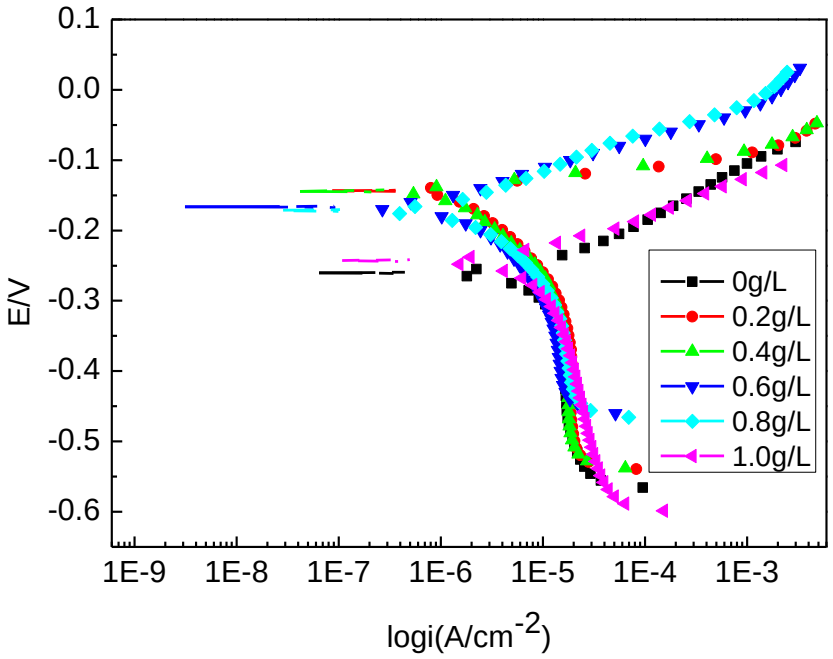

Figure 10. Polarization curves of the Ni-G composite coatings with different concentrations of graphene oxide prepared at 1.5 A/dm^2 in 3.5% NaCl solution.

Table 1. Fitting result of the polarization curve of composite coatings with different concentrations of graphene oxide

GO concentration (g/L)	b_a (mV)	b_c (mV)	i_{corr} (A/cm^2)	E_{corr} (V)
0	27	-40	2.06×10^{-6}	-0.261
0.2	12	-107	1.08×10^{-6}	-0.138
0.4	15	-104	9.43×10^{-7}	-0.139
0.6	43	-43	5.14×10^{-7}	-0.166
0.8	57	-62	9.49×10^{-7}	-0.174
1.0	41	-105	3.27×10^{-7}	-0.243

As shown in Fig. 11, after adding different concentrations of GO, the capacitive arc radius of the composite coating changes. When the graphene oxide concentration in the plating solution is 0, the capacitive arc radius of the coating is the smallest, and the corrosion resistance is the lowest. When the concentration of graphene oxide in the plating solution increases, the capacitive arc radius gradually increases, and the corrosion resistance improves. When the graphene oxide concentration is 0.6 g/L, the capacitive arc radius is the largest, and the coating has the best corrosion resistance. However, when the concentration of graphene oxide exceeds 0.6 g/L, the capacitive arc radius is significantly smaller, and the corrosion resistance of the coating weakens. In addition, according to the fitting data of the impedance spectrum in Table 2, when the concentration of graphene oxide is lower than 0.6 g/L, the capacitance of the passive film decreases with increasing graphene oxide concentration, and the charge transfer resistance (Rct) increases, which indicates that the thickness and density of the passive film increases, the number of surface voids decreases, and the corrosion resistance of the composite coating is gradually improved. When the concentration of graphene oxide exceeds 0.6 g/L, the charge transfer resistance and corrosion resistance of the composite coating decrease accordingly.

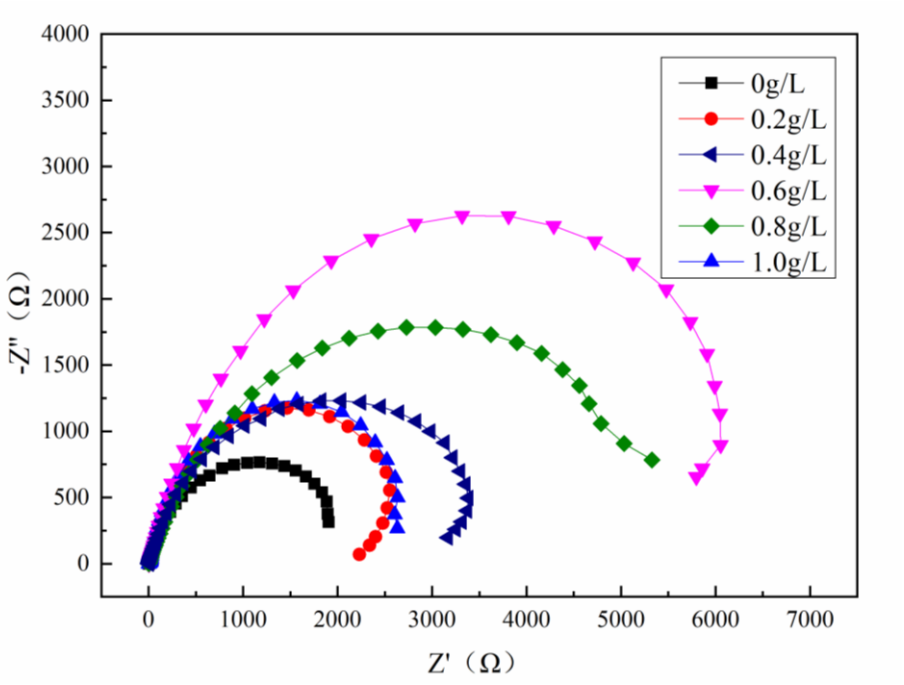

Figure 11. Nyquist plot of the Ni-G composite coatings with different concentrations of graphene oxide prepared at 1.5 A/dm^2 in 3.5% NaCl solution.

Table 2. Impedance spectrum fitting result of composite coatings obtained with different concentrations of graphene oxide

GO concentration (g/L)	R_s (Ω•cm^2)	Rct (Ω•cm^2)	CPE (Ω^{-1}•cm^{-2}•s^{-n})
0	3.743	2320	0.00016257
0.2	3.059	2877	0.00042866
0.4	4.321	3781	0.0011106
0.6	3.960	7010	0.00015312
0.8	3.194	5677	0.00020747
1.0	3.538	2969	0.0005019

4. CONCLUSION

Ni-G composite coatings were successfully prepared by pulse electrodeposition-reduced GO. The combination of FT-IR and Raman spectroscopy revealed the successful preparation and reduction of graphene oxide. The SEM and EDS results show that increasing the current density and rotation angle of cathode has positive effects on the electrodeposition of Ni-G, indicating that the mechanism of Ni-G composite electrodeposition is controlled by both an electrochemical mechanism and a mechanical

stirring mechanism. The electrochemical impedance spectrum and polarization curves of the composites show that the Ni-G composite exhibits better corrosion resistance than does the plain nickel coating.

ACKNOWLEDGEMENTS
The authors gratefully acknowledge the support from Fundamental Research Funds for the Central Universities (18CX05552A) and the Natural Science Foundation of Shandong Province (ZR2019MEE108).

DATA AVAILABILITY STATEMENT
The data that support the findings of this study are available from the corresponding authors upon reasonable request.

References

1. A. Singh, K.R. Ansari, D.S. Chauhan, M.A. Quraishi and S. Kaya, *Sustainable Chem. Pharm.*, 16 (2020) 10025.
2. K. Qiao, Y. Zeng, *Mater. Corros.*, 71 (2020) 1913.
3. M. Salman, K.R. Ansari, J. Haque, V. Srivastava, M.A. Quraishi and M.A.J. Mazumder, *J. Heterocycl. Chem.,* 57 (2020) 2157.
4. X. Zhong, T. Shang, C. Zhang, J. Hu, Z. Zhang, Q. Zhang, X. Yuan, D. Hou, D. Zeng and T. Shi, *J. Alloys Compd.*, 824 (2020) 153947.
5. J. Winiarski, W. Tylus, M.S. Krawczyk and B. Szczygieł, *Electrochim. Acta*, 196 (2016) 708.
6. L. Elias, A.C. Hegde, *Mater. Today:. Proc.*, 5 (2018) 3078.
7. S. Tian, K. Gao, H. Zhang, H. Cui and G. Zhang, *Trans. Indian Inst. Met.*, 73 (2020) 713.
8. Y. Gao, H. He, W. Tan, Y. Peng, X. Dai and Y. Wu, *Int. J. Hydrogen Energy*, 45 (2020) 6015.
9. S. Salomé, N.M. Pereira, E.S. Ferreira, C.M. Pereira and A.F. Silva, *J. Electroanal. Chem.*, 703 (2013) 80.
10. Y. Fan, Y. He, P. Luo, T. Shi and X. Chen, *J. Electrochem. Soc.*, 163 (2016) D68.
11. S. Kasturibai, G.P. Kalaignan, *Bull. Mater. Sci.*, 37 (2014) 721.
12. L. Elias, H.A. Chitharanjan, *Surf. Coat. Technol.*, 283 (2015) 61.
13. M. Refai, Z.A. Hamid, R.M. El-kilani and G.E.M. Nasr, *Chem. Pap.*, 75 (2021) 139.
14. F. Li, J. Cheng, S. Zhu, J. Hao, J. Yang and W. Liu, *Mater. Sci. Eng., A*, 682 (2017) 475.
15. L. Peng, Z. Xu, Z. Liu, Y. Guo, P. Li and C. Gao, *Adv. Mater.,* 29 (2017) 1700589.
16. T. Wang, B. Zhao, H. Jiang, H. Yang, K. Zhang, M.M.F. Yuen, X. Fu, R. Sun and C. Wong, *J. Mater. Chem. A,* 3 (2015) 2335.
17. C. Hsieh, J. Wei, J. Lin and W. Chen, *Catal. Commun.*, 16 (2011) 220.
18. H. Zeng, J. Wu, Y. Ma, Y. Ye, J. Liu, X. Li, Y. Wang, Y. Liao, X. Luo, X. Xie and Y. Mai, *ACS Appl. Mater. Interfaces*, 10 (2018) 41690.
19. M. Pumera, Z. Sofer, *Chem. Soc. Rev.*, 46 (2017) 4450.
20. X. Zhang, J. Cai, W. Liu, B. Huang and S. Lin, *J. Appl. Electrochem.*, 50 (2020) 713.
21. G. Riveros, M. León, D. Ramírez, L. Hernández, F. Martín, R. Romero and E.A. Dalchiele, *J. Electrochem. Soc.*, 167 (2020) 122508.
22. Y. Liu, F. Zheng, Y. Wu, C.C. Koch, P. Han, C. Zhang, Y. Liu and Y. Zhang, *J. Alloys Compd.,* 826 (2020) 154080.
23. D. Das, I. Noh, *Adv Exo Med Biol*, 1064 (2018) 3.
24. L. R. Safina, K.A. Krylova, *J. Phys. Conf. Ser.*, 1435 (2020) 12067.
25. J. Xie, L. Jiang, J. Chen, D. Mao, Y. Ji, X. Fu, R. Sun and C. Wong, *Chem. Eng. J.*, 393 (2020)

124598.
26. Y. Ji, J. Xie, J. Wu, Y. Yang, X. Fu, R. Sun and C. Wong, *J. Power Sources*, 393 (2018) 54.
27. C. Liu, F. Su and J. Liang, *Appl. Surf. Sci.*, 351 (2015) 889.
28. O.Y. Kurapova, I.V. Lomakin, S.N. Sergeev, E.N. Solovyeva, A.P. Zhilyaev, I.Y. Archakov and V.G. Konakov, J. Alloys Compd., 835 (2020) 155463.
29. X. Shen, J. Sheng, Q. Zhang, Q. Xu and D. Cheng, J. Mater. Eng. Perform., 27 (2018) 3750.
30. H. He, C. Gao, *Chem. Mater.*, 22 (2010) 5054.
31. A. Gupta, C. Srivastava, *J. Electroanal. Chem.*, 861 (2020) 113964.
32. D. Kuang, L. Xu, L. Liu, W. Hu and Y. Wu, *Appl. Surf. Sci.,* 273 (2013) 484.
33. Z. Xue, W. Lei, Y. Wang, H. Qian and Q. Li, *Surf. Coat. Technol.*, 325 (2017) 417.
34. M. Wang, Y. Niu, J. Zhou, H. Wen, Z. Zhang, D. Luo, D. Gao, J. Yang, D. Liang and Y. Li, *Nanoscale*, 8 (2016) 14587.
35. M. Diba, D.W.H. Fam, A.R. Boccaccini and M.S.P. Shaffer, *Prog. Mater Sci.*, 82 (2016) 83.
36. R.D. Noce, S. Eugénio, K.I. Siwek, T.M. Silva, M.J. Carmezim, A.M.P. Sakita, R.L. Lavall and M.F. Montemor, *Diamond Relat. Mater.*, 104 (2020) 107740.
37. N. Guglielmi, *J. Electrochem. Soc.*, 119 (1972) 1009.
38. S. Wang, W.J. Wei, *Mater. Chem. Phys.*, 78 (2003) 574.
39. P. Xiong-Skiba, D. Engelhaupt, R. Hulguin and B. Ramsey, *J. Electrochem. Soc.*,152 (2005) C571.
40. A. Lozano-Morales, E.J. Podlaha, *J. Appl. Electrochem.*, 25 (1995) 519.
41. D.W. Snaith, P.D. Groves, *Trans. IMF*, 55 (1977) 136.
42. D.W. Snaith, P.D. Groves, *Trans. IMF*, 56 (1978) 9.
43. S. Singh, S. Samanta, A.K. Das and R.R. Sahoo, Surf. Interfaces, 12 (2018) 61.
44. C. Thomsen, S. Reich, Phys. Rev. Lett., 85 (2000) 5214.
45. C. Guo, Y. Zuo, X.H. Zhao, J.M. Zhao and J.P. Xiong, Surf. Coat. Technol., 202 (2008) 3246.
46. A.A. Aal, K.M. Ibrahim and Z.A. Hamid, Wear, 260 (2006) 1070.
47. D.Z. Huang, L.D. Shen, J.S. Chen and J. Zhu, Trans. Indian Inst. Met., 67 (2014) 351.
48. A.A. Chernyshev, A.B. Darintseva, T.N. Ostanina, I.A. Panashchenko, A.A. Orlova, A.E. Novikov and A.S. Artamonov, Int. J. Hydrogen Energy,46 (2021) 0360.
49. M.R.A. Karim, S.A. Raza, E.U. Haq, K.I. Khan, A.A. Taimoor, M.I. Khan, M. Pavese and P. Fino, Appl. Phys. A, 172 (2021).
50. L.Y. Chen, Y.H. Tang, K. Wang, C.B Liu and S.L. Luo, Electrochem. Commun., 13 (2011) 133.
51. H. Wu, F. Liu, W. Gong, F. Ye, L. Hao, J. Jiang and S. Han, *Surf. Coat. Technol.*, 272 (2015) 25.
52. J. Chen, J. Li, D. Xiong, Y. He, Y. Ji and Y. Qin, *Appl. Surf. Sci.*, 361 (2016) 49.
53. C. Liu, K. Wang, S. Luo, Y. Tang and L. Chen, *Small*, 9 (2011) 1203.
54. C.L. Min, A.M. Zhong and M.M. Shuo, J. Rare Earths, 23 (2005) 403.
55. S. Zhang, F.H. Cao, L.R. Chang, J.J. Zheng, Z. Zhang, J.Q Zhang and C.N Cao, Appl. Surf. Sci., 257 (2011) 9213.